Meas. Sci. Technol. **10** (1999) 387–392. Printed in the UK PII: S0957-0233(99)99430-4

Complex permittivity of some ultralow loss dielectric crystals at cryogenic temperatures

Jerzy Krupka†, Krzysztof Derzakowski‡, Michael Tobar§, John Hartnett§ and Richard G Geyer‖

† Instytut Mikroelektroniki i Optoelektroniki PW, Koszykowa 75, 00-662 Warsaw, Poland
‡ Instytut Radioelektroniki PW, Nowowiejska 15/19, 00-665 Warsaw, Poland
§ Department of Physics, University of Western Australia, Nedlands, WA 6009, Australia
‖ National Institute of Standards and Technology, Radio Frequency Technology Division, 325 Broadway, Boulder, CO 80303, USA

Received 18 November 1998, in final form 3 February 1999, accepted for publication 15 February 1999

Abstract. Whispering gallery modes were used for very accurate permittivity and dielectric loss measurements of ultralow loss isotropic and uniaxially anisotropic single crystals. Several materials including sapphire, YAG, quartz, and $SrLaAlO_4$ were measured. The total absolute uncertainty in the real part of permittivity tensor components was estimated to be $\pm 0.1\%$, limited principally by the uncertainty in sample dimensions. Imaginary parts of permittivities were measured with uncertainties of about 10%, limited by the accuracy of Q-factor measurements of whispering gallery modes. It has been observed that, for most crystals, dielectric losses can be approximated by a power function of absolute temperature only in limited temperature ranges. At temperatures between 4–50 K, losses are often affected by impurities, which are always present in real crystals.

Keywords: complex permittivity, dielectric losses, whispering gallery modes, cryogenic measurements, microwave measurements, dielectric property measurements

1. Introduction

The whispering gallery mode method has proved to be one of the most accurate for measurements of complex permittivity of extremely low loss dielectrics. In early papers only the dielectric loss tangent was measured by this technique [1, 2]. Recently the WGM method was employed for very precise measurements of real pemittivity and dielectric losses of both isotropic and uniaxially anisotropic materials [3–5]. This method was also used in our measurements of ultralow loss single crystal materials including sapphire, yttrium alumina garnet (YAG), quartz, $SrLaAlO_4$ and in our already published measurements of rutile [6, 7].

2. Measurement procedure

The most effective way to eliminate conductor losses in accurate dielectric loss tangent measurements is to use higher-order azimuthal modes, called whispering gallery modes (WGMs), excited in cylindrical specimens of the material under test. In order to evaluate permittivity tensor components of a uniaxially anisotropic material, a cylindrical specimen must first be obtained that is oriented with the cylindrical axis along a principal direction of anisotropy. Then two WGM resonant frequencies of the specimen that exhibit quasi-TE (H-mode) and quasi-TM (E-mode) electromagnetic field structures are measured. Finally, the system of two nonlinear determinant equations is solved to evaluate permittivity tensor components. With known specimen permittivities, resonant frequencies for several other modes are computed and compared with experimental values to check the validity of mode identification. Detailed analysis of uncertainties in permittivity evaluation leads to the conclusion that the dominant part of the relative permittivity error is approximately double the relative error in the diameter of a cylindrical specimen. To ensure such permittivity uncertainty, resonant frequencies must be computed with uncertainties that are smaller than the dielectric resonator diameter uncertainty.

Once permittivities are found, dielectric loss tangents are evaluated as solutions to the equations

$$\left.\begin{aligned} Q_{(E)}^{-1} &= p_{e\perp}^{(E)} \tan\delta_\perp + p_{e\parallel}^{(E)} \tan\delta_\parallel + R_S/G^{(E)} \\ Q_{(H)}^{-1} &= p_{e\perp}^{(H)} \tan\delta_\perp + p_{e\parallel}^{(H)} \tan\delta_\parallel + R_S/G^{(H)} \end{aligned}\right\} \quad (1)$$

where $\tan\delta_\perp$ and $\tan\delta_\parallel$ are the dielectric loss tangents perpendicular and parallel to the anisotropy axis; $p_{e\perp}^{(H)}$, $p_{e\parallel}^{(H)}$, $p_{e\perp}^{(E)}$, $p_{e\parallel}^{(E)}$ are the electric energy filling factors perpendicular and parallel to the anisotropy axis of the resonant structure, for quasi-TM WGMs (superscript E) and

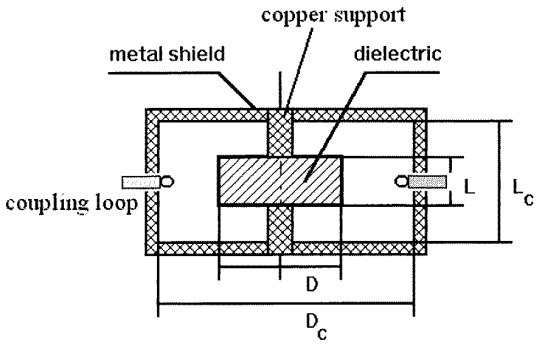

Figure 1. Whispering gallery mode fixture used in laboratory experiments.

quasi-TE whispering gallery modes (superscript H), and $G^{(E)}$ and $G^{(H)}$ are the geometric factors for quasi-TM and quasi-TE respectively. The geometric factors can be evaluated from the expression:

$$G = \frac{\omega \iiint_V \mu_0 \boldsymbol{H} \cdot \boldsymbol{H}^* \, \mathrm{d}v}{\oint\!\!\int \boldsymbol{H}_t \cdot \boldsymbol{H}_t^* \, \mathrm{d}s}. \qquad (2)$$

The resolution in loss tangent evaluation depends on geometric factor values. The larger the geometric factor, the higher the loss tangent resolution. In practice, for properly chosen azimuthal mode numbers and a sufficiently large metal shield, terms involving geometric factors can be neglected. In such a case dielectric loss tangent uncertainties are essentially the same as these in unloaded Q-factor measurements. For WGMs the shapes of resonant curves often differ from the shape of an ideal Lorentzian curve so, typically, loaded Q-factor uncertainties are about 10%. Hence similar uncertainties exist in loss tangent measurements as those in unloaded Q-factor determination. This is true if coupling is weak and insertion losses in scattering parameter measurements are properly accounted for.

In our measurements all samples were mounted at the centre of a copper cavity having two adjustable coupling loops positioned at two opposite sides of the symmetry plane of the cavity as shown in figure 1. Both loops were rotated 45° with respect to the plane of symmetry, in opposite directions to allow easy coupling to both quasi-TE and quasi-TM mode families. At room temperature, the coupling loops were adjusted symmetrically to obtain very weak coupling to higher azimuthal order modes (insertion loss below −60 dB). With decreasing temperature, the coupling coefficients increased due to significant unloaded Q-factor changes. At temperatures below 100 K insertion losses were typically in the range from −40 to −10 dB, and they were taken into account in unloaded Q-factor evaluations.

3. Results of real permittivity measurements

3.1. Sapphire

The sample was made of ultrahigh grade sapphire crystal. The sample had the following parameters.

- Sample size $D = 20.030 \pm 0.005$ mm; $L = 6.709 \pm 0.005$ mm.

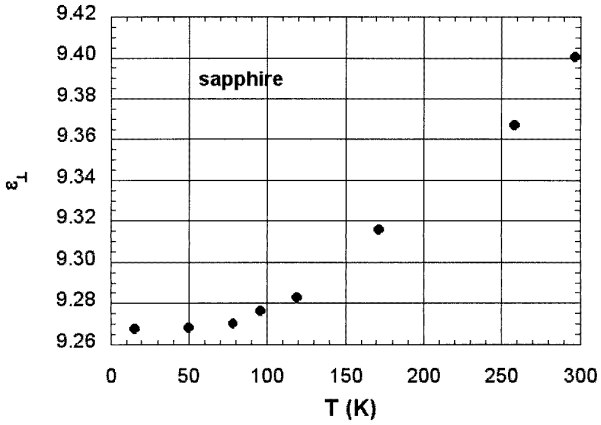

Figure 2. Permittivity component perpendicular to anisotropy axis versus temperature for sapphire.

Table 1. Intercomparison data for sapphire at room temperature.

$\varepsilon_\perp$	$\varepsilon_\parallel$	Frequency (GHz)	References
9.395 ± 0.004	11.589 ± 0.004	audio	[10]
$9.395 \pm 0.1\%$	$11.586 \pm 0.1\%$	8.3, 8.9	[5]
$9.399 \pm 0.2\%$	$11.553 + 2\%$[a]	13.6, 14.3	[9]
$9.400 \pm 0.1\%$	$11.587 \pm 0.1\%$	21.4, 21.7	This work
9.419 ± 0.004	11.662 ± 0.004	900	[11]
9.486 ± 0.004	11.806 ± 0.004	1800	[11]

[a] Permittivity affected by the presence of air gap between the sample and metal shield.

- Crystallographic structure: rhombohedral.
- Alignment of cylinder axis with the crystal optic axis: 20 min.
- Impurities: $<10^{-4}$.
- Thermal expansion coefficients at ambient temperature: along c-axis, 5.8×10^{-6} K^{-1}; perpendicular to c-axis, 5.06×10^{-6} K^{-1}.
- Copper enclosure size: $D_c = 36.0$ mm; $L_c = 21.85$ mm.

We used S1-9 (21.4 GHz) and N1-11 (21.7 GHz) WGMs for permittivity and the dielectric loss tangent determination. Several other modes, S1-7, S1-8, S1-10, N1-7, N1-8 and N1-9, were measured to check the validity of mode identification. The total absolute uncertainty in the real part of permittivity tensor components was estimated to be less than 0.1%. Thermal expansion coefficient changes versus temperature [8] were taken into account in permittivity evaluation. The results of permittivity measurements of sapphire are shown in figures 2 and 3. Sapphire is a frequently used dielectric at microwave frequencies and permittivity data are available in the literature for intercomparison (see some of them in table 1). Most of the data in table 1 are within 0.1% tolerance. At infrared frequencies both permittivity tensor components of sapphire increase with frequency, as shown in the last two rows of table 1.

One interesting question is the permittivity value of the sapphire specimen at the lowest measured temperature if no dimensional changes from room temperature values are accounted for. Analysis has shown that both permittivity components for sapphire at 15 K would be about 0.13%

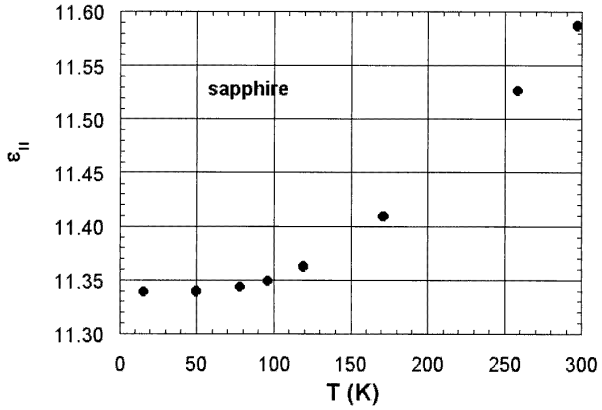

Figure 3. Permittivity component parallel to anisotropy axis versus temperature for sapphire.

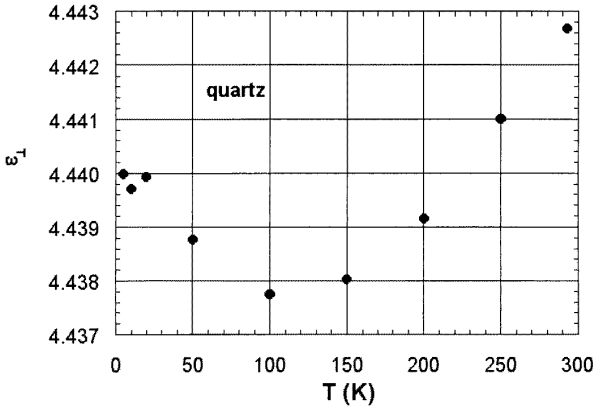

Figure 4. Permittivity component perpendicular to anisotropy axis versus temperature for quartz.

larger than their values at 15 K given in figures 2 and 3. For sapphire, relative permittivity uncertainty caused by neglecting expansion is therefore at least ten times smaller than the observed permittivity changes in the temperature range from 15 K to 300 K. The influence of thermal expansion is especially important at low temperatures when permittivity changes are small. Generally, as temperature decreases, thermal expansion coefficient values converge to zero. At temperatures between 4–20 K paramagnetic impurities often affect the measurement uncertainty of the real permittivity. Resonant frequency changes in this range primarily depend on the kind and amount of paramagnetic impurities [12]. Since permeability of the samples is assumed to be equal to unity in permittivity evaluations, data at very low temperatures represent an 'effective' permittivity.

3.2. Quartz

The sample had the following parameters.

- Sample size (at 295 K): $D = 49.88 \pm 0.01$ mm; $L = 32.23 \pm 0.01$ mm.
- Crystallographic structure: trigonal.
- Alignment of cylinder axis with the crystal optic axis: better than 1°.
- Impurities: $Al^+ < 30 \times 10^{-6}$; $Fe^+ < 10 \times 10^{-6}$; $Na^+ < 10 \times 10^{-6}$; $Li^+ < 5 \times 10^{-6}$; OH^-—present but not determined quantitatively.
- Thermal expansion coefficients at ambient temperature: along c-axis, 7.5×10^{-6} K^{-1}; perpendicular to c-axis, 13.7×10^{-6} K^{-1}.
- Copper enclosure size: $D_c = 80.0$ mm; $L_c = 50.0$ mm.

We used S2-14 (16.9 GHz) and S1-15 (17.2 GHz) WGMs for permittivity and the dielectric loss tangent determination. Several other modes: S1-12, S1-13, S1-14, S2-12 and S2-13, were measured to check the validity of mode identification. Results of permittivity measurements of quartz are shown in figures 4 and 5. Quartz is one of the most popular materials used in the electronics industry. Its material properties, including permittivity, have been measured by hundreds of researchers. Some permittivity measurement data for quartz taken from the literature are shown in table 2.

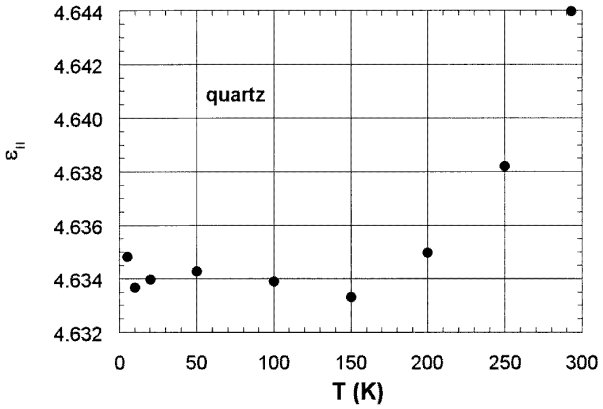

Figure 5. Permittivity component parallel to anisotropy axis versus temperature for quartz.

Table 2. Intercomparison data for quartz at room temperature.

$\varepsilon_{\perp}$	$\varepsilon_{\parallel}$	Frequency (GHz)	References
4.5208[a]	4.6368	audio	[10]
4.4348 ± 0.001	4.6368 ± 0.001	audio	[15]
4.43	4.5853	4.4, 5.0	[16]
$4.4430 \pm 0.2\%$	4.59 + 2%[b]	7.8, 9.0	[13]
$4.4427 \pm 0.1\%$	$4.6440 \pm 0.1\%$	16.9, 17.2	This work
4.430 ± 0.004	4.633 ± 0.004	35.0	[14]
4.4648 ± 0.004	4.6483 ± 0.004	900	[11]
4.4901 ± 0.004	4.6742 ± 0.004	1800	[11]

[a] This value was later corrected by the same authors in [15].
[b] Permittivity affected by the presence of air gap between the sample and metal shield.

Again, our measurements are in good agreement with the literature data presented, although there are a few published values (most of them not shown here) in which permittivities differ by a few per cent from the data shown in table 2. As quartz permittivity changes versus temperature are about one order of magnitude smaller than those for sapphire, they would be affected by uncertainties in thermal expansion coefficients. Uncertainties in thermal expansion coefficients, which we assumed in our permittivity computations, were not specified in [17] and [18]. At very low temperatures (4–20 K) permittivity values of quartz should be treated as 'effective'

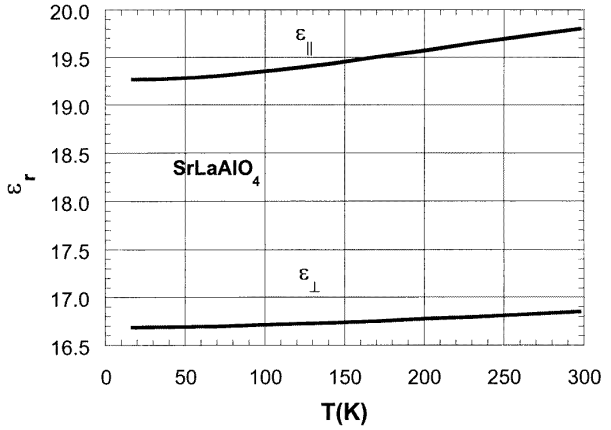

Figure 6. Permittivity components perpendicular and parallel to anisotropy axis versus temperature for $SrLaAlO_4$.

since permeability variations can be affected by the presence of paramagnetic impurities.

3.3. $SrLaAlO_4$

The sample had stoichiometry $SrLa_{1.03}Al_{0.97}O_4$ and the following parameters.

- Sample size: $D = 17.18$ mm; $L = 9.00$ mm.
- Crystallographic structure: tetragonal.
- Accuracy of alignment of cylinder axis with the crystal optic axis: better than 1^0.
- Impurities: $< 10^{-4}$.
- Thermal expansion coefficients at ambient temperature: along c-axis, 17.1×10^{-6} K^{-1}; perpendicular to c-axis, 7.55×10^{-6} K^{-1}.
- Copper enclosure size: $D_c = 36.0$ mm, $L_c = 21.85$ mm.

We used S1-5 (12.1 GHz) and N1-6 (11.8 GHz) WGMs for permittivity and dielectric loss tangent determination. Several other modes, S1-4, S2-4, S2-5, N1-4 and N1-5, were measured to check the validity of mode identification. The manufacturer provided thermal expansion coefficient data for this sample. For $SrLaAlO_4$, as for sapphire, relative permittivity uncertainty caused by neglecting thermal expansion is at least ten times smaller than observed permittivity changes in the temperature range from 15 K to 300 K. Permittivity measurement results for $SrLaAlO_4$ are shown in figure 6.

3.4. YAG

The sample was made of yttrium alumina garnet crystal and had the following parameters.

- Sample size (at 295 K): $D = 21.65 \pm 0.01$ mm; $L = 7.865 \pm 0.01$ mm.
- Crystallographic structure: cubic.
- Impurities: $<5 \times 10^{-5}$.
- Thermal expansion coefficient at ambient temperature: 6.9×10^{-6} K^{-1}.
- Copper enclosure size: $D_c = 36.0$ mm; $L_c = 21.85$ mm.

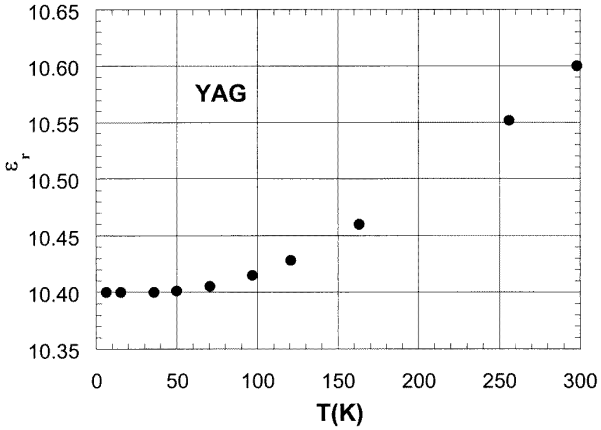

Figure 7. Permittivity versus temperature for YAG.

Table 3. Anisotropy ratio for various materials.

Material	Anisotropy ratio at 20 K	Anisotropy ratio at 300 K
Sapphire	1.224	1.232
Rutile [6, 7]	2.23	1.90
Quartz	1.044	1.045
$SrLaAlO_4$	1.16	1.18

We only used one WGM, namely S1-10 (20.2 GHz), for permittivity and dielectric loss tangent determination since the permittivity of YAG is isotropic due to the cubic crystallographic structure of this material. Several other modes, S1-7, S1-8, and S1-9, were measured to check the validity of S1-10 mode identification.

For the YAG sample, thermal expansion coefficient data were again provided by the manufacturer. In addition, the relative permittivity uncertainty caused by neglecting thermal expansion is at least ten times smaller than observed permittivity changes in the temperature range from 15 K to 300 K, similar to the situation for both sapphire and $SrLaAlO_4$. Permittivity measurement results for YAG are shown in figure 7.

3.5. Anisotropy ratio

All materials that were measured, except YAG, exhibited dielectric uniaxial anisotropy. The anisotropy ratio (ratio of permittivity component parallel to anistropy axis to permittivity component perpendicular to anisotropy axis) varies with temperature and is different for various materials as shown in table 3. Among the materials measured by us, rutile has the largest anisotropy ratio [6, 7] (2.23) and quartz the smallest (1.044) at 20 K.

4. Results of dielectric loss tangent measurements

Loss tangent measurement results are shown in figures 8–11. Computed contributions of copper wall losses at 15 K are given for the WGMs employed in the measurements and are indicated in the figure captions. Even for the lowest loss material (sapphire at 15 K), wall losses are at least 20 times smaller than the dielectric losses (note that $\tan\delta_\perp$ for

Table 4. Dielectric loss factors and dielectric loss–temperature exponents at 100 K.

f (GHz)	Material	$A_\perp$(100 K)	$A_\parallel$(100 K)	$K_\perp$(100 K)	$K_\parallel$(100 K)
21.3	Sapphire	5×10^{-16}	2×10^{-16}	4.5	4.5
20.2	YAG	1×10^{-12}		3.0	
17	Quartz	8×10^{-6}	5×10^{-6}	≈ 0	≈ 0
12	$SrLaAlO_4$	1.6×10^{-9}	4×10^{-9}	1.7	1.7
4.5	Rutile [6, 7]	3.2×10^{-11}	1.2×10^{-10}	2.7	2.7
9	Sapphire [5]	2×10^{-16}	8×10^{-17}	4.5	4.5
72	Sapphire [1]		8.2×10^{-16}		4.6
5	Rutile [19]	2.8×10^{-11}		2.7	

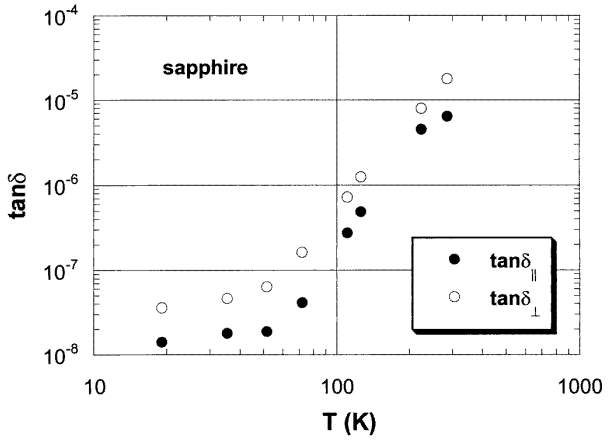

Figure 8. Dielectric loss tangent components perpendicular and parallel to anisotropy axis versus temperature for sapphire. $R_s/G = 1.5 \times 10^{-9}$ for S1-9 mode and 2.2×10^{-10} for N1-11 mode.

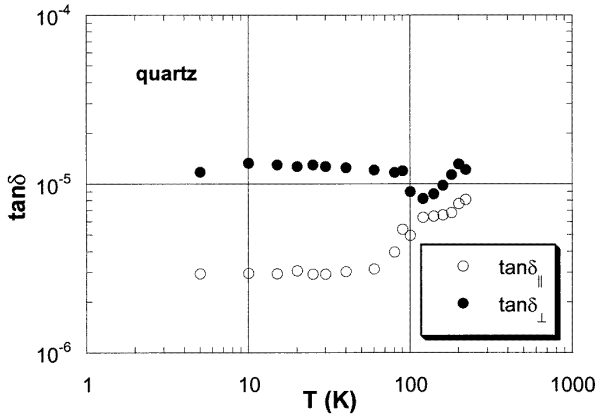

Figure 9. Dielectric loss tangent components perpendicular and parallel to anisotropy axis versus temperature for quartz. $R_s/G = 4.9 \times 10^{-10}$ for S1-15 mode and 6.5×10^{-9} for S2-14 mode.

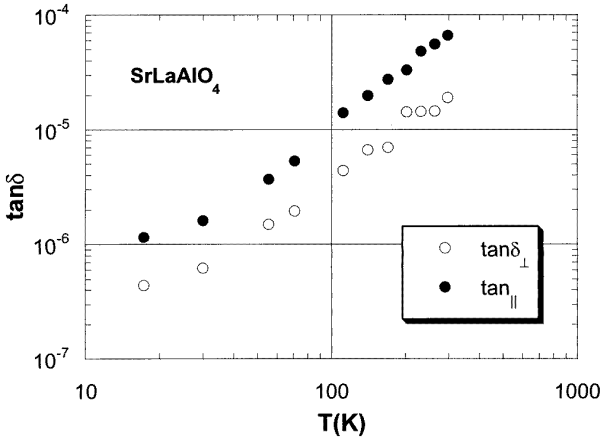

Figure 10. Dielectric loss tangent components perpendicular and parallel to anisotropy axis versus temperature for $SrLaAlO_4$. $R_s/G = 1.0 \times 10^{-8}$ for S1-5 mode and 5.5×10^{-9} for N1-6 mode.

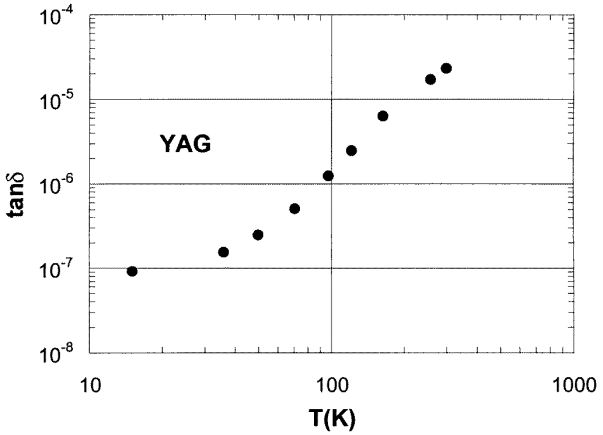

Figure 11. Dielectric loss tangent versus temperature for YAG. $R_s/G = 4.7 \times 10^{-10}$ for S1-10 mode.

sapphire depends 90% on the unloaded Q-factor of S1-9 mode). Therefore, loss tangent values should increase by no more than 5% if wall losses were to be completely neglected in all our measurements. We took conductor losses into account so that uncertainties in loss tangent determination were essentially the same as the uncertainties in the unloaded Q-factor measurements.

For all measured materials the dielectric loss tangent increases with temperature. The temperature at which the slope of the dielectric loss tangent versus temperature approaches a maximum on a logarithmic scale is about 100 K. At certain temperature ranges near 100 K dielectric losses can be approximated by power functions of absolute temperature:

$$\begin{aligned} \tan\delta_\perp &= A_\perp T^{K_\perp} \\ \tan\delta_\parallel &= A_\parallel T^{K_\parallel}. \end{aligned} \tag{3}$$

Dielectric loss factors and power exponents evaluated at 100 K for various materials are given in table 4, while table 5 lists dielectric loss tangents at 100 K. Data in the last four

Table 5. Dielectric losses at 100 K.

f (GHz)	Material	$\tan\delta_{\perp}$(100 K)	$\tan\delta_{\parallel}$(100 K)
21.3	Sapphire	5×10^{-7}	2×10^{-7}
20.2	YAG	1×10^{-6}	
17	Quartz	8×10^{-6}	5×10^{-6}
12	$SrLaAlO_4$	4×10^{-6}	1×10^{-5}
4.5	Rutile [6, 7]	8×10^{-6}	3×10^{-5}
9	Sapphire [5]	2×10^{-7}	8×10^{-8}
72	Sapphire [1]		1.3×10^{-6}
5	Rutile [19]	7×10^{-6}	

rows of tables 4 and 5 were taken from our earlier work or from the literature. In data intercomparison, one should note that dielectric losses are frequency dependent. For example, for sapphire, losses increase approximately linearly with frequency so the data measured at 21.3 GHz (first row) and 9 GHz (sixth row) are in very good agreement.

Some theoretical papers on dielectric losses in pure single crystals [e.g. 20] predict a temperature and frequency dependence for various crystal lattice structures. Our measurement data show that in real crystals losses exhibit more complex behaviour than that predicted by these theories, even over limited temperature ranges. For most crystals at very low temperatures losses are affected by impurities. In the other crystals such as quartz, piezoelectric effects can dominate the loss mechanism, although the influence of OH^- ions on the dielectric loss tangent in our quartz sample cannot be excluded.

5. Summary

The results presented in this paper establish a very accurate (within 0.1% tolerance) permittivity database versus temperature for a few ultralow loss crystals. The dielectric loss tangent data can also be treated as reference values for fixed frequencies. However, this is only true for a limited temperature range in which the specimens are not affected by unknown impurities. Over broad temperature ranges, losses in real crystals exhibit more complicated behaviour than that predicted by simplified theoretical models presented in the literature. In particular, power loss–temperature formulae describing dielectric loss can be applied only over limited temperature ranges. Further studies of various materials using the WGM technique are necessary. These would serve as experimental databases for engineers designing devices employing very low loss dielectrics and for physicists working on new theories to predict the complex permittivity of materials accurately. For most single crystal oxides the permittivity increases with temperature at temperatures above 100 K. An exception is rutile. For this reason rutile is an ideal material for the construction of composite thermally compensated dielectric resonators [21, 22] which have already found practical applications.

References

[1] Braginsky V, Ilchenko V S and Bagdassaro Kh S 1987 Experimental observation of fundamental microwave absorption in high quality dielectric crystals *Phys. Lett.* A **120** 300–5

[2] Dobromyslov V S and Kryukov A V 1993 Q value of shielded dielectric resonators *J. Commun. Technol. Electron.* **36** 125–32

[3] Krupka J, Derzakowski K, Abramowicz A, Tobar M and Geyer R G 1997 Measurements of the complex permittivity of extremaly low loss dielectric materials using whispering gallery modes *IEEE MTT Symp. (Denver) June 8–14* (Piscataway, NJ: IEEE) pp 1347–50

[4] Baker-Jarvis J, Geyer R G, Grosvenor J H Jr, Janecic M D, Jones Ch A, Riddle B, Weil C M and Krupka J 1998 Dielectric characterization of low-loss materials *IEEE Trans. Dielectric Electric. Insul.* **5** 571–7

[5] Krupka J, Derzakowski K, Abramowicz A, Tobar M and Geyer R G 1999 Use of whispering gallery modes for complex permittivity determinations of ultra-low loss dielectric materials *IEEE Trans. Microwave Theory Technol.* to be published

[6] Tobar M E, Krupka J, Ivanov E N and Woode R A 1998 Measurement of the complex permittivity of rutile between 10 to 300 Kelvin using whispering gallery modes *J. Appl. Phys.* **83** 1604–9

[7] Luiten A N, Tobar M E, Krupka J, Woode R, Ivanov E N and Mann A G 1998 Microwave properties of a rutile resonator between 2 and 10 K *J. Phys. D: Appl. Phys.* **31** 1383–91

[8] White G K 1993 Reference materials for thermal expansion: certified or not? *Thermochim. Acta* **218** 83–99

[9] Kobayashi Y and Senju T 1993 Resonant modes in shielded uniaxial-anisotropic dielectric rod resonators *IEEE Trans. Microwave Theory Technol.* **41** 2198–205

[10] Shelby R, Fontanella J and Andeen C 1980 The low temperature electrical properties of some anisotropic crystals *J. Phys. Chem. Solids* **41** 69–74

[11] Lowenstein E V, Smith D R and Morgan R L 1973 Optical constants for far infrared materials. I. Crystalline solids *Appl. Opt.* **12** 398–406

[12] Luiten A N, Mann A G and Blair D G 1996 Paramagnetic susceptibility and permittivity measurements at microwave frequencies in cryogenic sapphire resonators *J. Phys. D: Appl. Phys.* **29** 2082–90

[13] Geyer R and Krupka J 1995 Microwave dielectric properties of anisotropic materials at cryogenic temperatures *IEEE Trans. Instrum. Meas.* **44** 329–31

[14] Jones R G 1976 The measurement of dielectric anisotropy using open microwave resonator *J. Phys. D: Appl. Phys.* **9** 819–27

[15] Fontanella J, Andeen C and Schuele D 1974 Low-frequency dielectric constant of alpha-quartz, sapphire, MgF_2 and MgO *J. Appl. Phys.* **45** 2852–4

[16] Wolf I and Schwab N 1980 *Messung der Dielektrizitatszahl anisotroper dielektrischer Materialien im Mikrowellenbereich* (Opladen: Westdeutscher)

[17] White G K 1964 Thermal expansion of silica at low temperatures *Cryogenics* **4** 1–7

[18] Swenson C A, Roberts R B and White G K 1985 *Thermophysical Properties of Some Key Solids (CODATA Bulletin 59)* ed G K White and M L Minges (Oxford: Pergamon) ch 4

[19] Klein N, Zuccaro C, Dahne U, Schultz H and Tellmann N 1995 Dielectric properties of rutile and its use in high temperature superconducting resonators *J. Appl. Phys.* **78** 6683–6

[20] Gurevich V L and Tagantsev A K 1986 Intrinsic dielectric loss in crystals: low temperatures *Sov. Phys.–JEPT* **64** 142–51

[21] Klein N, Scholen A, Tellmann N, Zuccaro C and Urban K W 1996 Properties and applications of HTS-shielded dielectric resonators: a state-of-the-art report *IEEE Trans. Microwave Theory Tech.* **44** 1369–73

[22] Tobar M E, Krupka J, Ivanov E N and Woode R A 1997 Dielectric frequency temperature compensated whispering gallery mode resonators *J. Phys. D: Appl. Phys.* **30** 2770–5